Int J Adv Manuf Technol (2016) 86:1113–1125
DOI 10.1007/s00170-015-8149-0

ORIGINAL ARTICLE

Effect of grinding wheel ultrasonic vibration on chip formation in surface grinding of Inconel 718

Sisi Li[1] · **Yongbo Wu**[2] · **Mitsuyoshi Nomura**[2]

Received: 8 August 2015 / Accepted: 23 November 2015 / Published online: 5 January 2016

Abstract Understanding the chip formation is one of most important issues in controlling the grinding wheel performance or the work surface finish in grinding process. This article discusses the effects of the ultrasonic vibration and peripheral speed of grinding wheel on the chip size and geometry in ultrasonic assisted grinding (UAG) of Inconel 718 with an electroplated cBN grinding wheel. Firstly, scanning electron microscopic (SEM) observations were performed on the chips formed at different vibration amplitudes and wheel peripheral speeds. The obtained 3D SEM images were used to determine the length and cross-section area of chips. Then, the geometries of chips were observed with SEM. The obtained results demonstrated that (1) chip size and geometry were distinctly affected by the ultrasonic vibration of grinding wheel but hardly by the wheel peripheral speed, e.g., the cross-section area of chips became smaller by 64.3 % and the length decreased by 36.3 %, respectively, once the ultrasonic vibration with an amplitude of $A_{p\text{-}p}$=9.4 μm has been imposed to the grinding wheel; (2) the UAG is potentially avoiding the formation of shear chips and prefers the flow chips, especially at larger amplitude; (3) little changes were found on the chip geometry as the wheel peripheral speed increased in UAG; (4) the change in the chip size and geometry caused by the ultrasonic vibration was supposed to be owing to the ultrasonic lubrication and the vibration in the rake angle of grain cutting edge.

Keywords Ultrasonic assisted grinding · Inconel 718 · Chip geometry · Ultrasonic lubrication · Rake angle

✉ Yongbo Wu
wuyb@akita-pu.ac.jp

Sisi Li
jjjjyyzzzz@gmail.com

Mitsuyoshi Nomura

[1] Graduate School, Akita Prefectural University, 84-4 Aza Ebinokuchi Tsuchiya, Yurihonjo, Akita 015-0055, Japan

[2] Department of Machine Intelligence and Systems Engineering, Akita Prefectural University, 84-4 Aza Ebinokuchi Tsuchiya, Yurihonjo, Akita 015-0055, Japan

1 Introduction

Inconel 718 is excellent at its mechanical properties such as good tensile, fatigue, creep, and rupture strength; this results in its use in a wide range of applications [1–3]. It is reported that nickel-based alloys account for over half of the materials used in the turbine industry, and aero engines utilize a large quantity of Inconel 718 material [4]. In the turbine components manufacturing, although the near net-shape methods such as castings, isothermal forging, and 3D-printing have been introduced in recent years, removing materials through machining operations is still the main method for achieving the desired accuracy and surface finish of the final parts [5]. Today, most aerospace engines, turbine discs, and blades made of Inconel 718 are conventionally machined by turning, cutting, and milling [6–8]. Compared with most materials, machining Inconel 718 is usually associated with high machining costs and low productivity, which make it be identified as "difficult-to-machine materials" [9, 10]. Furthermore, it is hard for these conventional machining processes to attain a fine surface finish and accurate dimensions [11].

Grinding, a special machining process with thousands of irregular cutting edges interacting with the workpiece simultaneously at a high speed, has been widely used in order to get good surface quality and high dimensional accuracy of workpieces. During grinding, each of the abrasive grains removes a

tiny amount of material from the workpiece. This removal mode contributes to improving the work surface finish and the form/dimension accuracy even for difficult-to-machine materials such as titanium [12]. Unfortunately, the grinding of Inconel 718 usually results in the excessive tool wear and thus the shortened tool working life, the decreased material removal rate (MRR) and the poor surface quality [13] because of the severe friction between the abrasive crystals and the workpiece which generates a considerable amount of heat and further make tool-workpiece interact condition be worse.

Against these problems, several techniques have been developed to decrease the friction and improve the grindability [14–16], e.g., vibration-assisted grinding, enhanced cooling techniques, and development of grinding wheels with higher performance. Among them, as a promising grinding technique, ultrasonic assisted grinding (UAG) has attracted great attention for decades for the sake of smaller grinding force, higher material removal rate, better surface quality, longer grinding wheel working life, and lower grinding heat generation due to a fundamental alteration in process kinematics [17]. However, most of researches on UAG have ever focused mainly on the hard-brittle materials such as crystal silicon and ceramics [18] and few researchers but D. Bhaduri et al. [19, 20] implemented their studies on UAG of nickel-based alloys. According to D. Bhaduri et al., UAG yields lower grinding forces, but a rougher work surface compared to conventional grinding (CG).

Meanwhile, the majority of published works on UAG can be broadly divided into two subcategories in terms of that the vibration affects either the grinding wheel performance or the work-surface finish [21]. The ability to control the grinding wheel performance or the work surface finish depends on our understanding of the chip formation. The chips formed during grinding are relatively small, and their sizes vary due to the randomly oriented cutting edges on the grinding wheel [22]. Under this condition, the chip formation mechanism causes a substantial increase of grinding forces. In addition, according to Liu et al. [23], analysis of chip morphology is a simple way to decide whether the grinding process is thermally out of control or not.

As literature reviewed above, the chip formation process is a subject widely studied. However, the chip formation behavior in UAG is still unclear, and no research has focused on the relation between the chip morphology and the ultrasonic vibration in particular involving Inconel 718. In this paper, aiming at the complete understanding of the chip formation in the UAG of Inconel 718, an experimental setup of performing ultrasonic-assisted surface grinding with cBN grinding wheel was established firstly, then the effects of the vibration amplitude and the wheel peripheral speed on the size and geometry of chips formed were systematically investigated by observing the geometries of the chips formed at different conditions and measuring their 3D dimensions using a SEM with 3D measurement function. The effect of the ultrasonic vibration on the chip size, chip geometry, and grinding forces is experimentally investigated. Finally, the formation mechanism of the chips with different sizes and geometries is discussed from the view points of the ultrasonic lubrication and the ultrasonic impact of grains on the chips.

2 Processing principle and experimental details

2.1 Processing principle

The processing principle of UAG is schematically illustrated in Fig. 1; a grinding wheel with a diameter of d_s attached on an ultrasonic spindle is ultrasonically vibrating at a frequency of f and a peak-to-peak amplitude of $A_{p\text{-}p}$ along its own axis (x-axis) and is rotated clockwise at a peripheral speed of V_c around its own axis. A plate-shaped workpiece is located below the wheel. Once a depth of cut Δ is given between the wheel and the workpiece, and the workpiece is fed rightward in y-direction at a feed rate of V_w, an UAG operation is performed. In this process, thus, a complicated relative motion of the abrasive grain on the work surface is generated owing to the combination of three kinds of local motion: rotation around wheel axis, work feed in y-direction, and vibration along wheel axis.

2.2 Experimental setup

Based on the above described processing principle, an experimental setup was constructed by installing a commercially available ultrasonic spindle (URT40 by Takesho Co., Ltd) onto an existing NC grinder (GRIND-X IGM15EX by Okamoto Machine Tool Works Co., Ltd.) via a 3-components piezoelectric dynamometer (9256A by Kistler Co., Ltd.) as displayed in Fig. 2. The dynamometer was located under the ultrasonic spindle and used for detecting grinding forces. An electroplated cBN grinding wheel was screwed on the left end face of the ultrasonic spindle, of which the abrasive grain mesh number was 140# and the diameter was 8 mm. A plate-shaped specimen of Inconel 718 with dimensions of 48×36×3 mm was used as the workpiece. In experiments, the Inconel 718 specimen was fixed on a work-holder under which a z-stage is located for determining the wheel depth of cut Δ.

2.3 Experimental conditions and procedure

As the purpose of this work is predominantly to investigate the effect of the wheel ultrasonic vibration on the

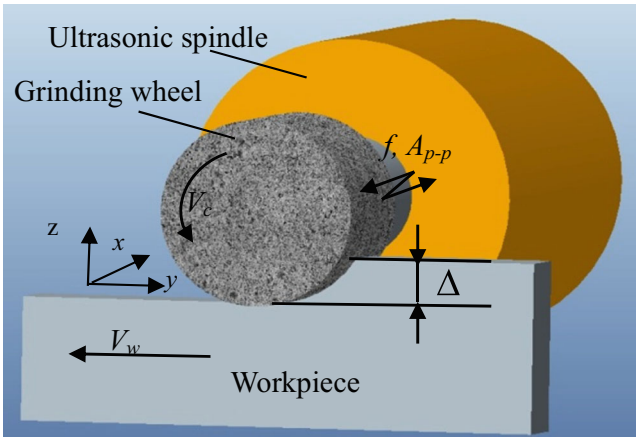

Fig. 1 Schematic illustration of processing principle of UAG

chip formation in UAG of Inconel 718, a model commonly used for discussing the material removal mechanism in CG of metal materials is employed to consider the chip formation behavior in this work as shown in Fig. 3. In this model, several assumptions and simplifications have been made as below.

- The cBN grains are rigid cone of the same size.
- Workpiece material is rigid plastic.
- The cBN grains located on the wheel working surface have the same height, and all of them take part in cutting during UAG.
- The volume of material removed by a grain in UAG is approximately equal to the intersection volume between the grain and the workpiece.

The grinding wheel is applied to the work material at a given wheel speed, a work feed rate, and a wheel depth of cut (Fig. 3a) to perform a up-cut grinding operation. As a cutting edge, the cone-like abrasive grain A with a half vertical angle θ (Fig. 3b) cuts into the work material and subsequently leads to the formation of a chip with the maximum

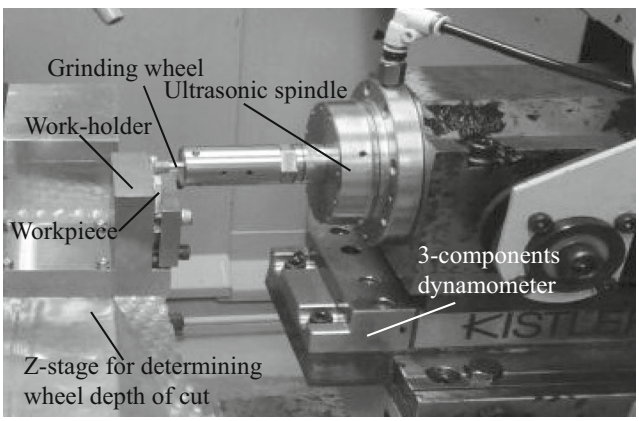

Fig. 2 The main portion of the experimental setup

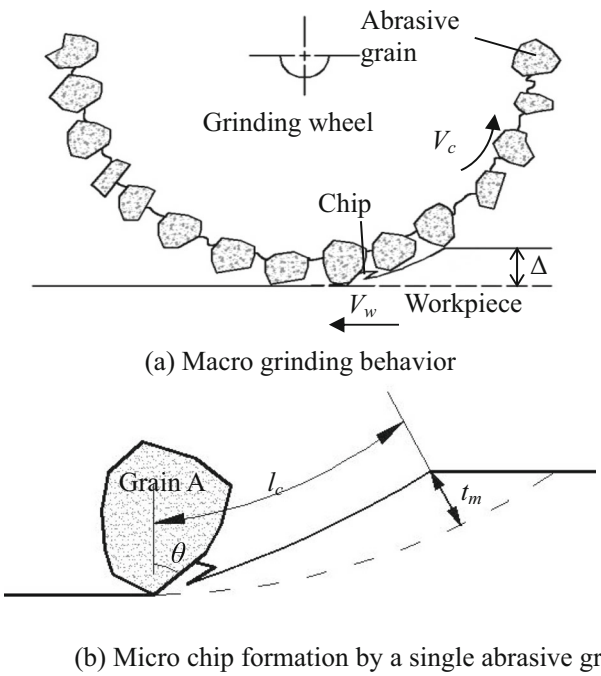

Fig. 3 Chip formation model in grinding. **a** Macro grinding behavior and **b** micro chip formation by a single abrasive grain

undeformed thickness of t_m and length of l_c; both the thickness and length can be expressed as:

$$t_m \approx 2\delta \frac{V_w}{V_c}\sqrt{\frac{\Delta}{d_s}} \quad (1)$$

$$l_c \approx \sqrt{\Delta d_s} \quad (2)$$

respectively, where δ is the successive cutting-point spacing [24, 25].

Generally speaking, a smaller value of t_m results in a lower cutting force and a better heat dissipation, indicating that the undeformed chip thickness t_m is an important index in grinding process. By contrast, the undeformed chip length l_c is dominantly related to the wheel wear [26]. Hence, in this paper, the effect of t_m was taken into discussion whereas the l_c was kept constant. According to Eqs. (1) and (2), there are several ways to change the value of t_m, e.g., the adjustment of wheel peripheral speed V_c, wheel depth of cut Δ, work feed rate V_w, and wheel diameter d_s, but the wheel depth of cut Δ and the wheel diameter d_s affect the l_c too. Therefore, the wheel depth of cut Δ and the wheel diameter d_s were kept constant in this work. Among the rest of the grinding parameters, i.e., V_c and V_w, the V_c is in inverse proportion to t_m, meaning the t_m is more sensitive to the wheel peripheral speed V_c compared with V_w. Typically, cBN abrasives require a speed of over 50 m/min for grinding Inconel 718 [27]. Thus, the wheel depth of cut Δ, the work feed rate V_w,

and the wheel vibration frequency f were set at Δ= 78.4 μm, V_w=15 mm/min, and f=40 kHz, while the wheel peripheral speed V_c and the wheel vibration amplitude $A_{p\text{-}p}$ were varied in the ranges of V_c=100.5–138.2 m/min and $A_{p\text{-}p}$=0–9.4 μm, respectively, as exhibited in Table 1. In addition, dry grinding operations were performed without coolant supplying. Three output variables of chip size, chip geometry, and grinding force were measured and observed.

An electron scanning microscope (SEM) with 3D measurement/observation functions (ERA-8900 by ELIONIX Co., Ltd.) was employed to measure the 3D chip size and observe the chip geometry. As an example, a part of chips typically formed at $A_{p\text{-}p}$=9.4 μm and V_c= 100.5 m/min were observed, and their 3D sizes were measured with the SEM. Figure 4a, b shows the obtained 2D and 3D SEM images of the chips, and Fig. 4c exhibits the 3D image of a single grain #1 (Fig. 4b) and its 3D size of a=25 μm, b=16 μm, and c=8 μm, respectively.

However, it is difficult to answer the question only from the SEM image that which one of dimensions a, b, c stands for the length or width or thickness of the chip. In surface grinding, the undeformed chip length is in general larger than its width and thickness considerably, and consequently, one of the three dimensions a, b, c which is maximum could be identified as the actual length of the chip formed. This fact could be confirmed if the thickness and length of the undeformed chip have been obtained by substituting the process parameters of V_w, V_c, Δ, d_s, and δ in Eqs. (1) and (2), respectively. Among these parameters, V_w, V_c, Δ, and d_s are the already known ones under the given grinding conditions (Table 1), however, the successive cutting point spacing δ is unknown. Therefore, for determining the δ, the distances δ_i (i=1,2,…, N) between the two neighbored grains along the grinding direction on the working surface of employed wheel were measured as shown in Fig. 5a, and 100 measurements, i.e., N=100, are as shown in Fig. 5b. It can be seen in Fig. 5b that although the value of δ_i varied in the range of 20–180 μm, more than half of them were in the range of 60–70 μm, and hence, the average value can be obtained as δ=65.52 μm.

Subsequently, substituting the currently obtained value of δ and the required process parameters tabulated in Table 1 into Eqs. (1) and (2) yielded the undeformed chip thickness of t_m=1.38 μm and its length of l_c=800 μm. Then, the maximum width b_m of the undeformed chip can be determined by Eq. (4) in the case of assuming the abrasive grains on the wheel working surface are cone-shaped with a half vertical angle of θ, and the cross section of the undeformed chip is the same as that of the grain owing to the replication principle as shown in Fig. 6.

$$b_m = 2t_m \tan\theta \tag{4}$$

In order to check if the assumption is true, the abrasive grains on the working surface of the wheel employed were observed by 3D SEM. Figure 7a, b shows the 3D SEM images of an arbitrary area of 1.5×1.5 mm on the wheel working surface and a typical grain A, respectively. It was found that most of the grains exhibited cone-shaped and the vertical angles of the grain A in yz- and xz-plane were 123 and 112°, respectively. Further, around 100 grains were randomly selected for measuring their vertical angles 2θ, and eventually, the percentage distribution was obtained as shown in Fig. 7c. It can be seen that although the values of 2θ either in xz-plane or in yz-plane varied in the range of 110–170°, over 60 % of them were 140–150°, resulting in the mean values of 2θ in xz- and yz-plane were 146 and 145°, respectively. Thus, the mean value of 2θ=146° in xz-plane was used for calculating b_m using Eq. (4). Eventually, in the experimental conditions in the current work, the undeformed chip width of b_m= 3.27 μm was obtained.

The above-mentioned results demonstrated that the undeformed chip length is considerably larger than its width and thickness, implying that the dimension of a (Fig. 4c) can be identified as the actual length of the chip formed. However, it is still hard to distinguish which one of b and c stands for the width and the thickness because there is a little difference between the thickness t_m and the width b_m according to aforementioned calculation results of t_m= 1.38 μm and b_m=3.27 μm. Fortunately, in grinding process, the dominant grinding characteristics (e.g., force and temperature) can generally be characterized with the chip cross-section area rather than its width or thickness. Therefore, the cross-section area was calculated using the measured dimensions of b and c and the vertical angle of 2θ whereas the chip length was obtained directly by measuring the largest dimension of a; in practice, the

Table 1 Experimental conditions

Workpiece	Inconel 718, L48×W36×T3 mm
Grinding wheel	Electroplated cBN#140, ϕ8×L8 mm (FSK 140)
Ultrasonic vibration	Frequency f=40 kHz
	Amplitude $A_{p\text{-}p}$=9.4, 7.7, 5.8, 4.1, 2.2, 0 μm
Process parameters	Workpiece feed rate V_w=15 mm/min
	Wheel peripheral speed V_c=100.5, 113.0, 125.6, 138.2 m/min
	Grinding width b=3 mm
	Grinding wheel depth of cut Δ=80 μm
Coolant	Without (dry grinding)

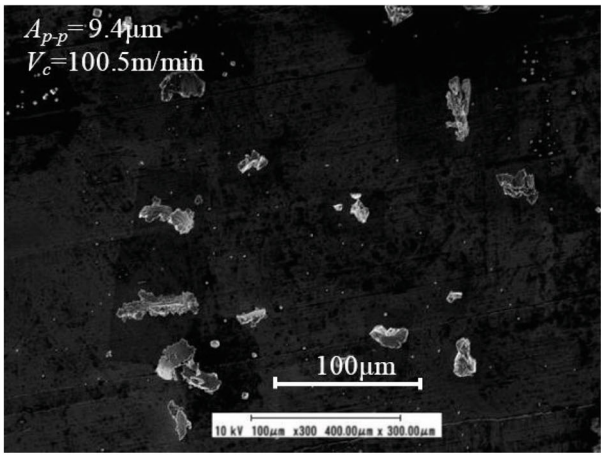

(a)

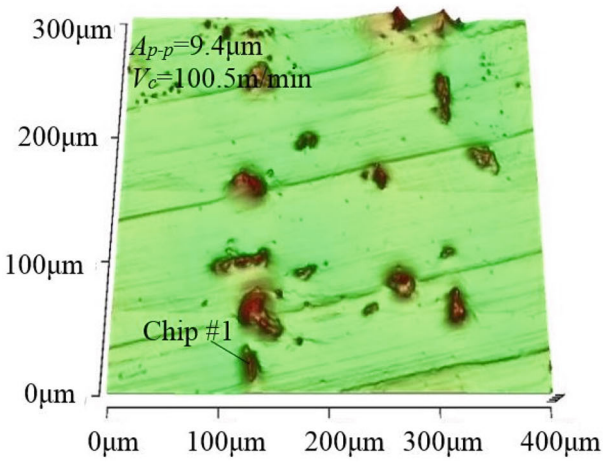

(b)

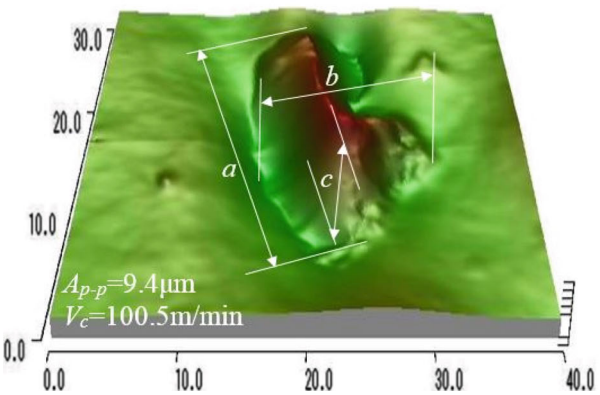

(c) a=25 μm, b=16 μm, c=8 μm

Fig. 4 Typical chips obtained: **a** 2D SEM images; **b** 3D SEM images; **c** 3D SEM image of a single chip

SEM images of chips were filtered, extracted, and binarized by using the commercial available Image-Pro Plus software to calculate the length and cross-section area of the chips.

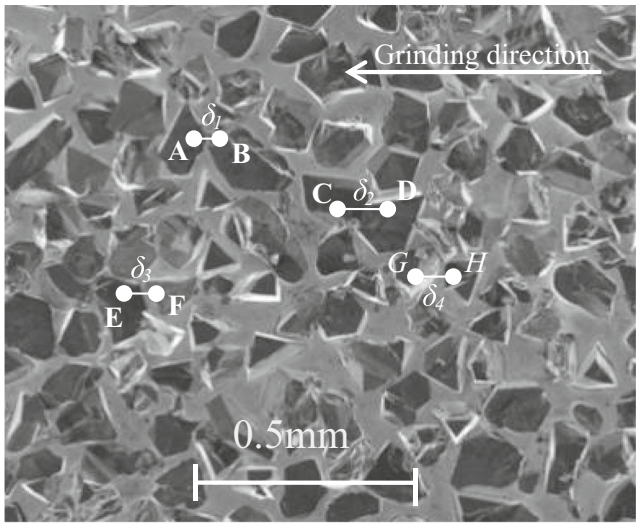

(a)

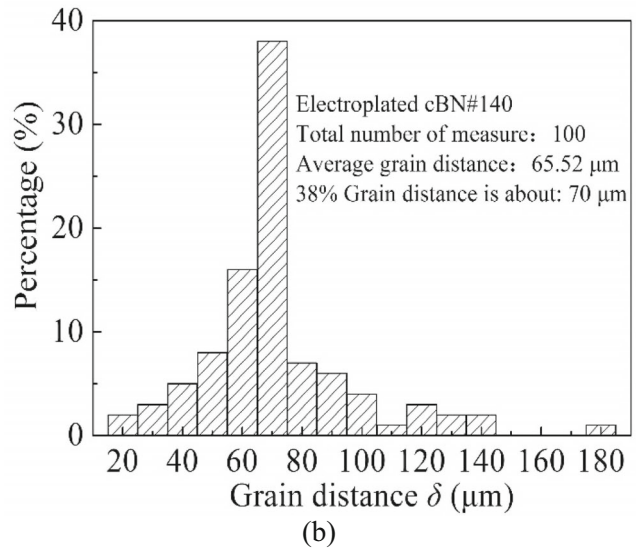

(b)

Fig. 5 The measurement of average grain distance in grinding direction: **a** 2D SEM image of grains; **b** measured grain distance percentage distribution

3 Experimental results

3.1 Chip size

Figure 8a, b shows the 3D SEM images of chips formed in UAG ($A_{P\text{-}P}$=9.4 μm) and CG at V_c=138.2 m/min, respectively. The majority of chips in UAG seem smaller than those in CG. Subsequently, 50 chips formed in each test were properly collected, and their 3D SEM images were obtained to achieve their sizes (lengths and cross-section areas). As a result, the chip length and its cross-section area at different vibration amplitudes for various wheel peripheral speeds were obtained as shown in Fig. 8c, d, respectively, where the error bars indicate the size variations of 50 chips in the corresponding test with the same grinding conditions. It is evident in Fig. 8c that

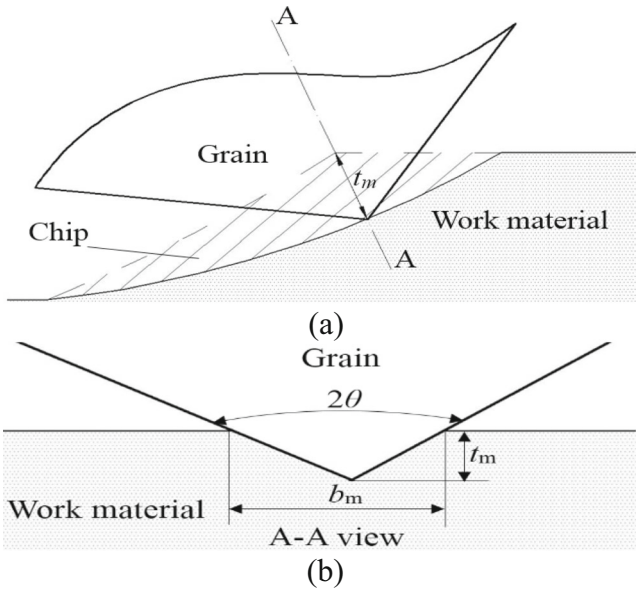

Fig. 6 Schematic drawing of the undeformed chip dimensions by a single abrasive grain in grinding

both the mean length and the mean cross-section area of 50 chips were decreased monotonously with the increasing vibration amplitude. It is further worthy to note that the cross-section area of chips became smaller by 64.3 %, and the mean length decreased by 36.3 %, respectively, once the ultrasonic vibration with an amplitude of $A_{p\text{-}p}$=9.4 μm has been imposed to the grinding wheel. Shifting the attention to the effect of the wheel peripheral speed (Fig. 8d) revealed that the cross-section area either in UAG or in CG decreased slightly with the increasing peripheral speed; however, the effect of the speed on the chip length either in UAG or in CG was not obvious. In a word, the chip size is distinctly affected by the ultrasonication but little effect of wheel peripheral speed was observed. Given that in grinding the normal force acting on the grain cutting edge rake face is increased with the increasing contact area between the chip and the cutting edge [28], and the grain cutting force is proportional to the chip cross-section area [25], these experimental observations on chip size imply that the grinding force would be reduced as the ultrasonic vibration amplitude increases.

3.2 Chip geometry

As revealed by Pei-Lum Tso [29], in conventional grinding of Inconel 718, the formed chips can be in general classified into six types, i.e., flow, shear, rip, knife, slice, and melt. In the present work involving the same workpiece, although all the six types of chips were also observed, the great majority of them were the shear, knife, and flow types either in UAG or in CG as typically shown in Fig. 9. Shifting the attention to the number percentages of each type under different grinding conditions, it can be found from Fig. 10 that the majority of chips

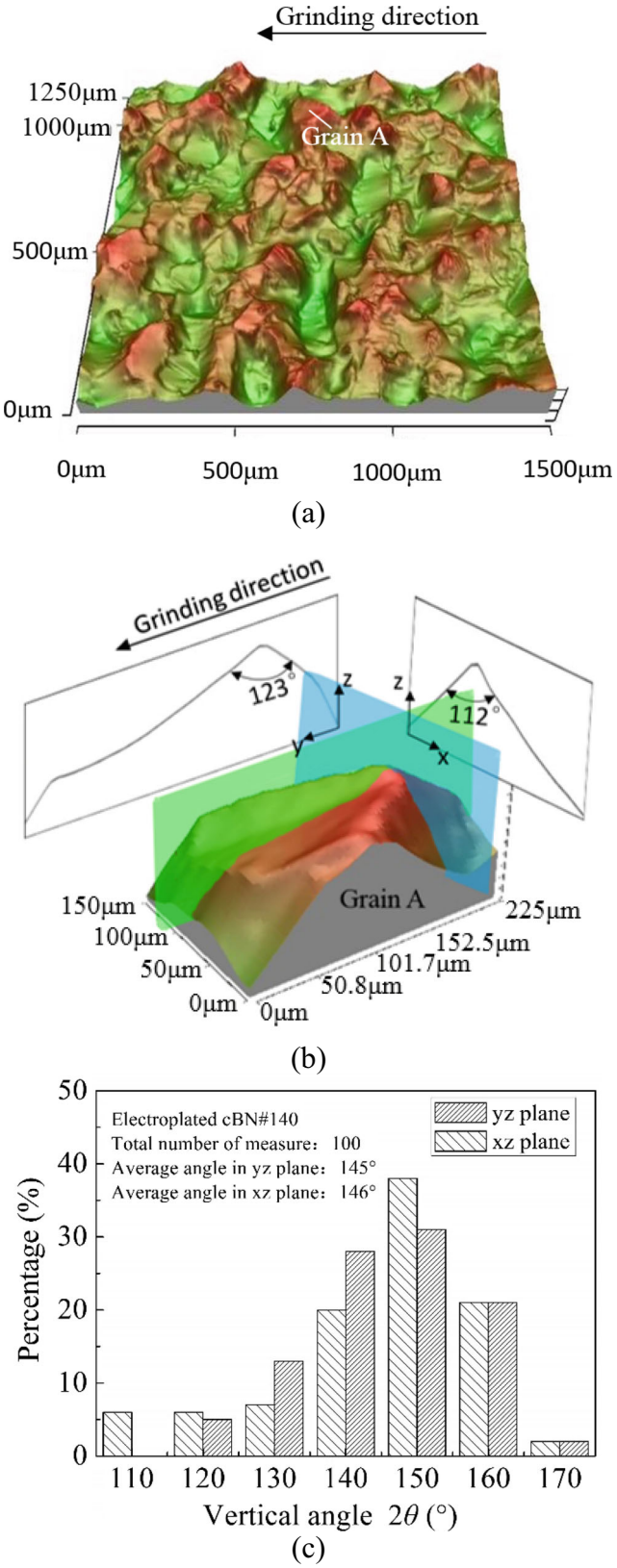

Fig. 7 The measurement of grain half vertical angle: **a** 3D SEM observation of grains; **b** cross-section of a typical grain A; **c** percentage vs. vertical angle

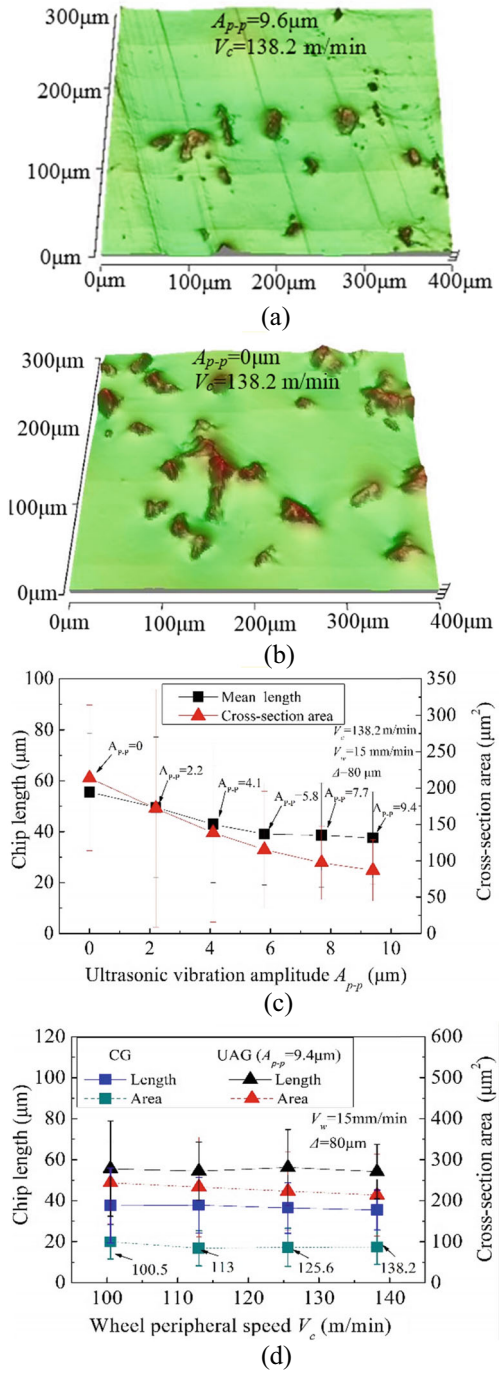

Fig. 8 Effects of ultrasonic vibration amplitude and wheel peripheral speed on chip size: **a** 3D SEM images of chips in UAG at $A_{p\text{-}p}$= 9.4 μm, **b** 3D SEM images of chips in CG, **c** chip lengths and cross-section area vs. vibration amplitude, **d** Chip lengths and cross-section area vs. wheel peripheral speed

in CG were shear type, whereas most of them in UAG were flow type especially at larger vibration amplitude ($A_{p\text{-}p} \geq$ 4.1 μm). This indicates that the UAG of Inconel 718 is potentially avoiding the formation of shear chips and prefers the flow chips especially at larger amplitude.

As for the effect of the wheel peripheral speed V_c, it can be found from Fig. 11 that in CG at the beginning as the V_c increased from 100.5 to 113 m/min, the percentage of the flow chip rapidly rose from 4 to 63 %, and little change can be found on the percentage of knife chip, while that of the shear chips dropped considerably from 86 to 30 %, and then as the V_c continued to increase, significant variations cannot be observed on the percentages of all the three types of chips. However, in UAG, little changes can be found on the percentages of all the three types of chips as the V_c increased from 100.5 to 138.2 m/min. These facts revealed that in CG of Inconel 718, the wheel peripheral speed would affect the chip formation significantly, whereas in UAG the chip formation is hardly affected by the wheel peripheral speed. The reason for these differences will be discussed in next section.

4 Discussion

4.1 Chips size

As afore-revealed in Section 3.1, the great majority of chips formed in UAG were smaller than those in CG. In order to find the reason why the ultrasonication resulted in the formation of smaller chips, the cutting traces of a single grain with and without ultrasonication in the grinding zone and the formation behavior of a chip by the grain are considered as illustrated in Fig. 12a, b, respectively.

In CG without ultrasonication (Fig. 12a), the grain's cutting trace is a 2D curved line in the *yz*-plane and the undeformed chip length is supposed to be equal to the length of the cutting trace, whereas in UAG, the cutting trace is a 3D curved line that looks like a spatial sinusoidal curve, and its length would be longer than that in CG, indicating that the undeformed chip length in UAG would be longer than that in CG. One of the present authors presented in his earlier work [30] on the UAG of SUS440C steel that the materials removed by a single abrasive grain with ultrasonication equals that without ultrasonication and thus the longer cutting trace results in the smaller cross-section area of chip. This would be one of the reasons why the cross-section area of chips in UAG is smaller than that in CG. Meanwhile, the ultrasonic vibration benefits the reduction of the friction coefficient between the grain and the chip and the ground work-surface for the sake of the so-called ultrasonic lubrication [31]; the larger the vibration amplitude is, the smaller the friction coefficient becomes, leading to the increase in shear angle and eventually decrease the chip thickness. This might be one of the reasons why the chip cross-section area decreased with the increasing ultrasonic vibration amplitude.

Figure 12b illustrates the instantaneous chip formation behavior at a moment in UAG. Although the ultrasonic vibration is purposely imposed on the grinding wheel along the wheel

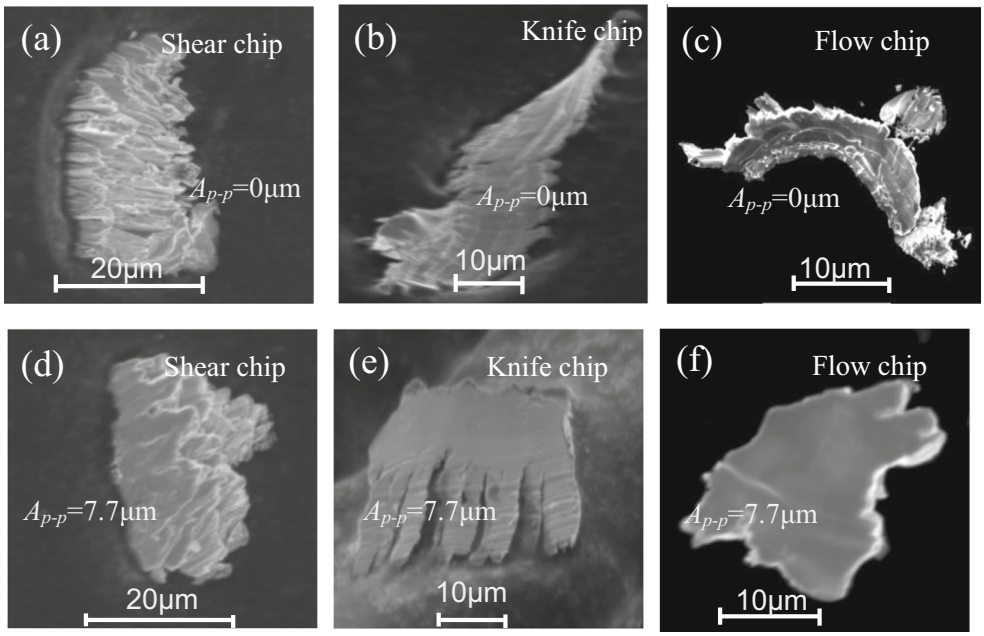

Fig. 9 Type of chips at Δ=80 μm and V_c=138.2 m/min: **a** shear chip in CG; **b** knife chip in CG; **c** flow chip in CG; **d** shear chip in UAG; **e** knife chip in UAG; **f** flow chip in UAG

axis (*x*-direction), usually it also occurs in the wheel radial direction owing to the LR transferring effect [32]. In the current work, for confirming this issue, the radial and axial ultrasonic vibration of the wheel was measured using a laser Doppler vibrometer (LV-1610 by Onosokki), and the obtained results indicated that the actual vibration amplitude in the radial direction (A_r) was about 0.4 μm whereas about 9.4 μm in the axial direction. Therefore, even the amplitude in the radial direction was much smaller than that in the axial direction, the impact effect of the ultrasonically vibrating grain takes place in the radial direction and the chip breakage is promoted, resulting in the formation of shorter chips compared with that in CG without the impact effect. This might be one of the reasons why the chips length in UAG was smaller than that in CG.

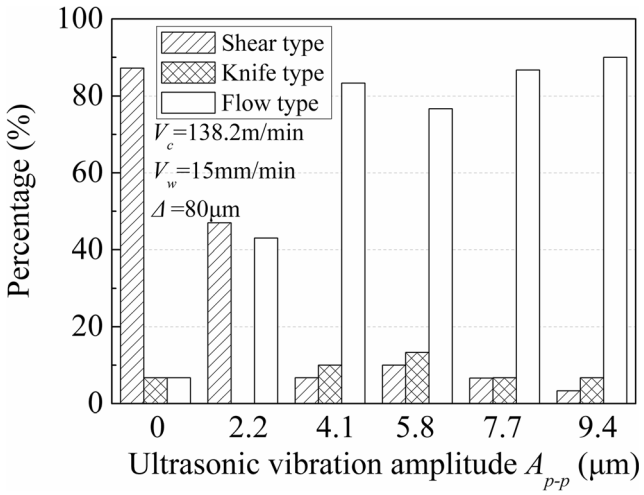

Fig. 10 Effect of vibration amplitude on chip type

4.2 General mechanism of chip formation

The generally accepted mechanism of chip formation in grinding is that of extrusion-like action [25] as shown in Fig. 13a. Between points A and C, grain and workpiece are just in contact without cutting action. At the very first stage of the interaction between grain and workpiece, plastic deformation occurs, the temperature rises, and normal stress exceeds the yield stress. The work material is abruptly sheared as it crosses the primary shear zone along the shear plane A–D that is determined by the shear angles φ. When the shear angle φ is small, the material in the front of grain is predominantly deformed and piled up due to shearing action, which is more relevant to high compressive stress, leading to the formation of a shear chip (Fig. 13b). The material piled up in the front of grain partially flows under the cutting edge, resulting in the generation of many cutting marks on the chip surface, which was frequently observed in the CG of Inconel 718 [33]. This kind of chips will bring a large specific grinding force, increase the grinding temperature, and cause serious grain wear.

The formation mechanism of flow chip is similar with that of shear chip, but the shear angle φ is larger compared with that in shear chip formation (Fig. 13c). When the shear angle is large, the flow chip formed with a narrow primary shear zone. In this case, there is low residual stress, and practically all of the energy consumed ends up in the chips instead of workpiece. In addition, the material is removed with a low strain and the contact condition turns into sliding. This phenomenon can be observed by scanning the chip grinding surface (Fig. 9c, f), which is smoother than shear chip (Fig. 9a, d).

The knife chip is formed frequently with fracture micro defects in work material (Fig. 13d). This kind of chips was

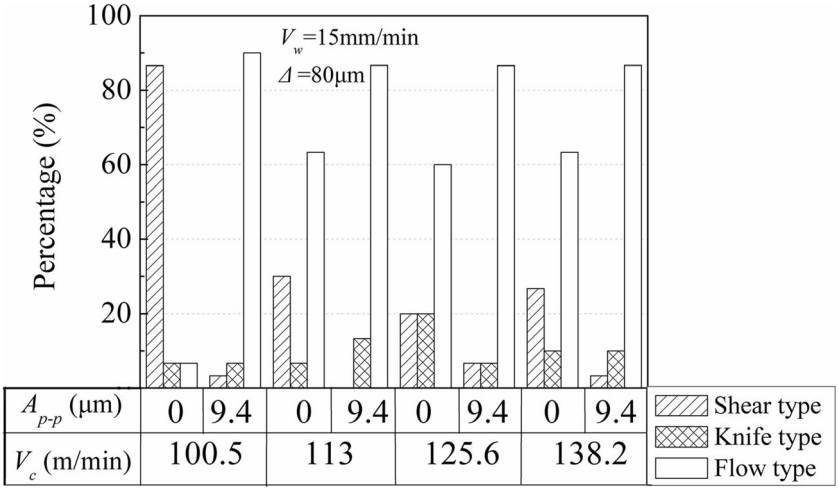

Fig. 11 Effect of wheel peripheral speed on chip type

actually found to occur when a relatively large depth of cut was applied [34]. This phenomenon brings a serious compressive force and ends up the occurrence of high compressive stress in the primary deformation zone, eventually inducing compressive residual stresses in the machined surfaces [35]. Due to the high compressive residual stress, the subsequently passing grain leads to fracture micro defects below the surface. This is the reason why the knife chip was formed with crack, as shown in Fig. 9b, e.

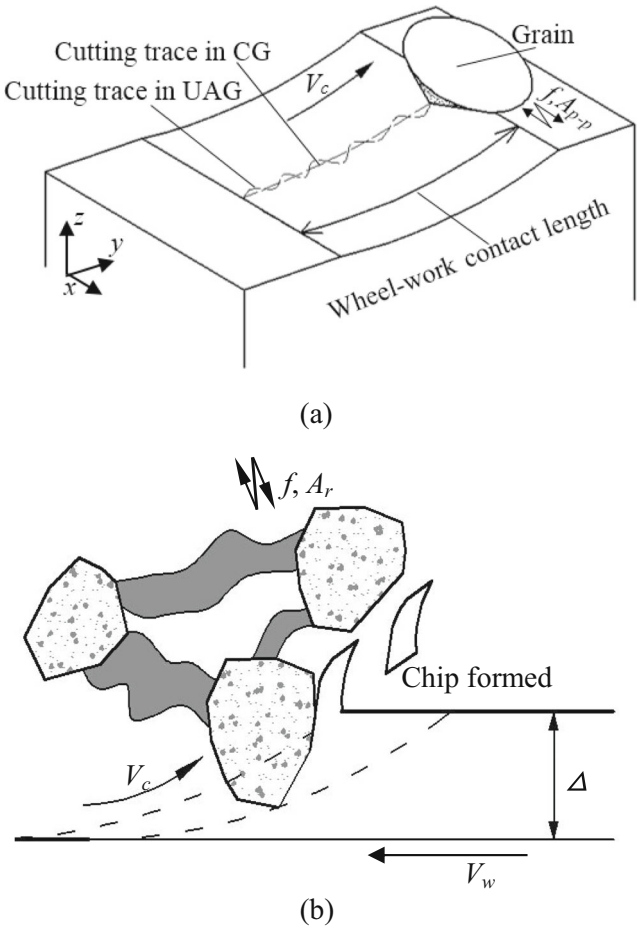

Fig. 12 **a** Grain cutting traces and **b** impact effect of grain on chip in UAG

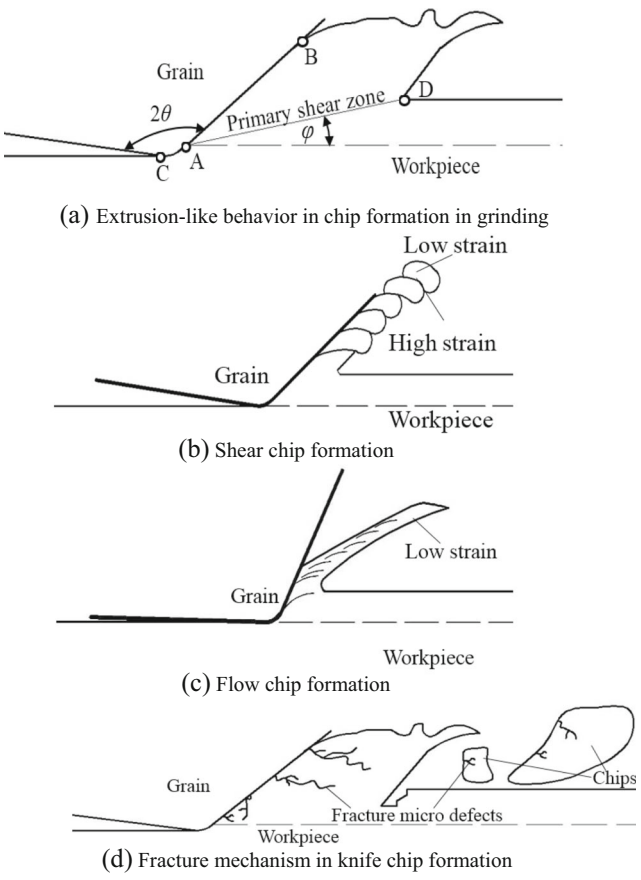

Fig. 13 Shear and fracture of chip in single grain. **a** Extrusion-like behavior in chip formation in grinding, **b** shear chip formation, **c** flow chip formation, **d** fracture mechanism in knife chip formation

4.3 Effect of ultrasonic vibration on chip geometry

Armarego and Brown [36] concluded that the shear angle φ is independent of both the grain width of cut and the chip thickness and can be determined by Eq. (5).

$$\tan(\varphi + \beta) = \cot\alpha \tag{5}$$

where β is the friction angle and determined by the friction coefficient μ_g between the rake face of cutting edge and the chip through the relationship of $\tan\beta=\mu_g$ and α is the rake angle of cutting edge. In CG, the angle α is usually the same with the half vertical angle θ of the grain; hence, it can be figured out from Eq. (5) that as long as the grinding is performed with a given grinding wheel at a given wheel depth of cut, the α will be a given constant, consequently the φ would increases as the β decreases. Elena Teidelt [31] pointed out that the ultrasonic vibration benefits the reduction of the friction coefficient μ_g; the larger the vibration amplitude is, the smaller the friction coefficient becomes, implying that larger vibration amplitude leads to a larger shear angle φ according to Eq. (5). This is considered to be one of reasons why the formation of flow chips was promoted by the ultrasonication of wheel, in particular, at larger amplitude.

For convenience, the 3D spatial cutting trace is redrawn on a 2D $l_c ox$ plane, which is fixed on the workpiece as in Fig. 14. A sinusoidal cutting trace is generated on the work surface due to the grain vibration velocity V_x in the wheel axis (x-direction) and the grinding speed V_l along the contact arc where the V_l and the V_x can be expressed as:

$$V_l(t) = V_c + V_w \tag{6}$$

$$V_x(t) = \pi f A_{p\text{-}p}\cos(2\pi f t) \tag{7}$$

It can be figured out from Eqs. (6) and (7) that the direction of the real grain cutting speed V varies in a sinusoidal pattern and quantitatively is indicated by the engagement angle γ determined by Eq. (8):

$$\gamma = \tan^{-1}\left(V_x \Big/ V_l\right) \tag{8}$$

Under the experimental conditions in the current work, the max value of V_x was similar with the value of V_l, resulting in the γ will oscillated in the range of −27 ($-\gamma_{max}$) to 27 ($+\gamma_{max}$). It is also inferred from Eqs. (6)–(8) that the engagement angle increases as the vibration amplitude increases. Thus, the chip hardly forms in same plastic deformation during a vibration cycle. Hence, the ultrasonic vibration eliminates the accumulation of chip compressive stress and makes the flow chip form easily. Meanwhile, flow chip formation leads to a low compressive residual stresses of chip, which make the formed chip break easily under the impact from the vibrating grain in plane zl.

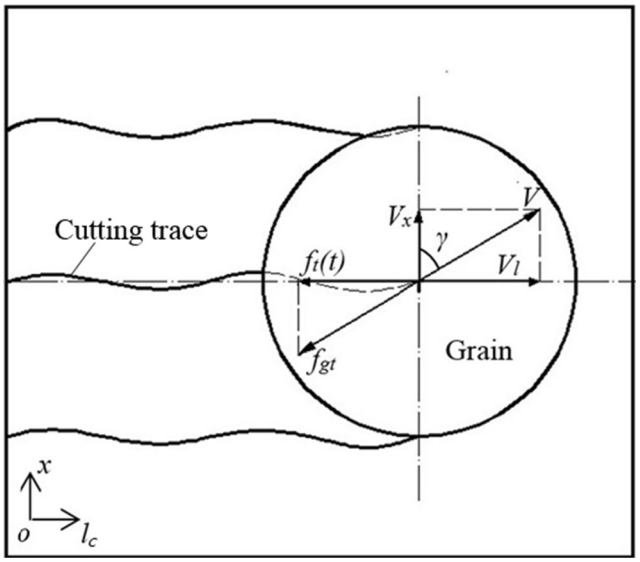

Fig. 14 Cutting trace in grinding zone and grinding forces on the grain in UAG

4.4 Grinding forces and specific grinding energy

As afore-discussed, with the assistance of ultrasonication, the shear angle φ is increased and the formation of flow chips is promoted. For confirming this issue, it is perfect to directly measure the shear angle; however, this is an extremely difficult task in fact. Therefore, given the grinding force is the function of the shear angle [37], the effect of the ultrasonic vibration on the grinding force is considered as below in order to indirectly measure the shear angle in the absence and presence of ultrasonication.

As shown in Fig. 14, the direction of the tangential grinding force f_{gt} acting on the grain cutting edge along the real grain cutting speed V is determined with the engagement angle γ and thus oscillates between $-\gamma_{max}$ and $+\gamma_{max}$ during one cycle of vibration during grinding. Thus, the instantaneous tangential grinding force $f_t(t)$ at time t along the wheel-workpiece contact arc l can be expressed as:

$$f_t(t) = f_{gt}\cos\gamma \tag{9}$$

Following the oscillation of γ, the $f_t(t)$ varies periodically, and its time-averaged value over one cycle with the period of T, f_t, is obtained by:

$$f_t = \frac{1}{T}\int_0^T f_t(t)dt = \frac{1}{T}\int_0^T f_{gt}\cos\gamma dt \tag{10}$$

By substituting Eqs. (1)–(8) into Eq. (10), and letting the number of the active grain cutting edges in the grinding zone

be N_g, the total time-averaged tangential grinding force F_t can be calculated by Eq. (11)

$$F_t = \frac{N_g}{T}\int_0^T f_{gt}\frac{V_c + V_w}{\sqrt{4\pi^2 f^2 A_{p\text{-}p}\cos^2(2\pi f) + (V_c + V_w)^2}}dt \tag{11}$$

Equation (11) indicates that the grinding force in UAG (i.e., $A_{p\text{-}p}>0$) would be smaller than that in CG (i.e., $A_{p\text{-}p}=0$), and in particular, the force F_t would be decreased as the ultrasonic vibration amplitude $A_{p\text{-}p}$ increases but linearly increases with the increase in the wheel peripheral speed of V_c.

To confirm this issue, grinding forces were measured under various values of $A_{p\text{-}p}$ and V_c. In practice, the F_t approximately equals the component of grinding force in y-direction (see Fig. 1) F_y, and hence, the F_y was experimentally obtained. Also, the component F_z in z-direction was measured for comparison. Figure 15a, b shows the obtained effects of the $A_{p\text{-}p}$ and the V_c on the two components of grinding force. Evidently, either the F_y or the F_z monotonously decreased as the $A_{p\text{-}p}$ increased (Fig. 15a), and almost linearly decreased with the increasing V_c (Fig. 15b). It should be noticed, for example, that at V_c=138.2 m/min, once the ultrasonic vibration at $A_{p\text{-}p}$= 9.4 μm has been applied, the values of F_y and F_z were dropped by 51.9 and 38.6 %, respectively, compared with that without ultrasonication ($A_{p\text{-}p}$=0 μm). These results agreed well with those predicted by Eq. (11) qualitatively as well as the implication made previously in Section 3.1. In addition, considered that the normal grinding force F_z is directly related to the occurrence of fracture micro defects on the chip by which the knife chip is characterized, the great reduction of the F_z owing to the ultrasonication might be one of the reasons why the number percentage of the knife chips in UAG was lower than that in CG (see Figs. 10 and 11). Also, the grinding force ratio of F_z/F_y was obtained as exhibited in the same Fig. 15, showing that the ratio increased with the increasing ultrasonic vibration amplitude $A_{p\text{-}p}$ (Fig. 15a), whereas little effect of the wheel peripheral speed V_c can be observed on the ratio (Fig. 15b) either in CG or in UAG. As revealed by Dong Kun Zhang [38], the larger grinding force ratio indicates that the grinding process mainly involves the friction ploughing and the deformation of chip is small. The obtained results shown in Fig. 15a accordingly demonstrated that the ultrasonic vibration indeed contributed to the occurrence of the friction ploughing and the reduction in chip deformation. This would in turn result in the reduction in grinding energy consumption; in other word, in the case of the same specific grinding energy consumption, a greater material removal rate, i.e., a higher grinding efficiency, would be achieved at a larger vibration amplitude.

Furthermore, the specific grinding energy in UAG was compared with that in CG. As the specific grinding energy is

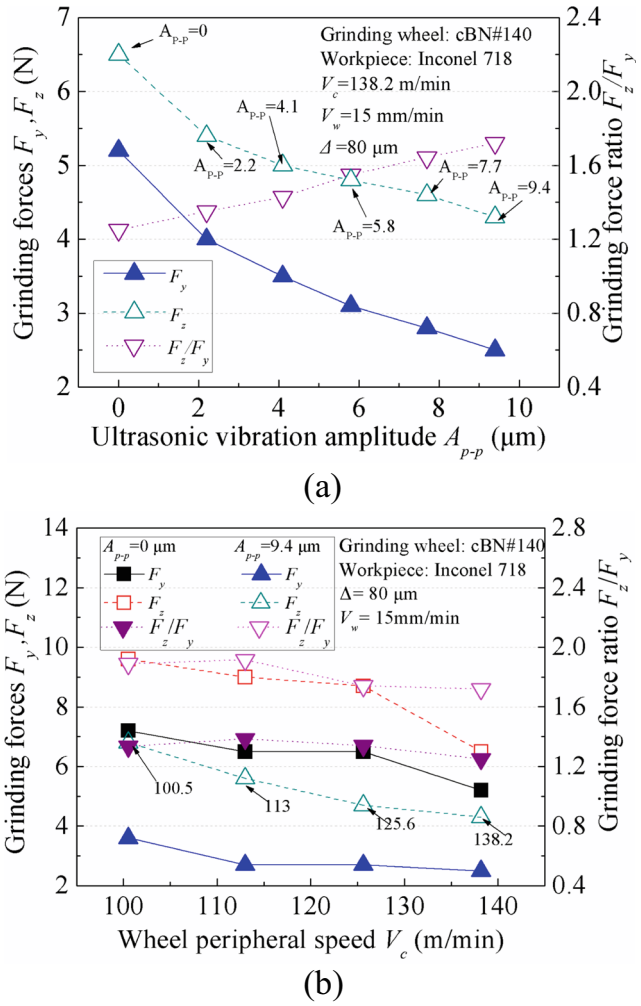

Fig. 15 Effects of **a** vibration amplitude and **b** wheel peripheral speed on grinding forces and grinding force ratio

defined as the energy per unit volume of material removed [25], in CG without ultrasonication, the specific grinding energy u can be expressed by following equation:

$$u = F_y V_c \Big/ 1000 b \Delta V_w \tag{12}$$

where F_y (N) is the tangential grinding force, V_c (m/min) is the wheel grinding speed, b (mm) is the grinding width, Δ (mm) is the wheel depth of cut, and V_W (m/min) is the workpiece feed rate. On the other hand, the specific grinding energy in UAG would be:

$$u = \left(F_y V_c + F_x V_x\right) \Big/ 1000 b \Delta V_w \tag{13}$$

where F_x (N) is the grinding force in x-direction due to the wheel ultrasonic vibration and V_x (m/min) is the wheel ultrasonic vibration speed determined by Eq. (7); both of them are varied periodically at the frequency of f during grinding.

In the current work, the values of V_c, b, Δ, and V_w have been already known as exhibited in Table 1 and that of F_y is

Table 2 V_x, F_x, F_xV_x, and F_yV_c typically obtained at V_c=138.2 m/min for various values of $A_{p\text{-}p}$

$A_{p\text{-}p}$ (mm)	0	$2.2*10^{-3}$	$4.1*10^{-3}$	$5.8*10^{-3}$	$7.7*10^{-3}$	$9.4*10^{-3}$
V_x (m/min)	0	−16.6~16.6	−30.9~30.9	−43.7~43.7	−58.0~58.0	−70.8~70.8
F_x (N)	0	−0.1~0.1	−0.1~0.1	−0.1~0.1	−0.1~0.1	−0.1~0.1
F_xV_x	0	0~1.66	0~3.09	0~4.37	0~5.8	0~7.08
F_yV_c	718.6	552.8	483.7	428.4	387.0	345.5

also the already known one as shown in Fig. 15. Then the F_x was actually measured with the same dynamometer used for F_y and F_z, and the value of V_x was calculated by substituting the f and $A_{p\text{-}p}$ given in Table 1 into Eq. (7). Table 2 exhibits the results typically obtained at V_c=138.2 m/min for various values of $A_{p\text{-}p}$. It can be seen that in a vibration cycle of wheel, the F_xV_x varied from 0 to the respective peek values for different $A_{p\text{-}p}$ while the F_yV_c decreased as the $A_{p\text{-}p}$ increased.

Subsequently, substituting the data shown in Table 2 and the values of b, Δ, and V_w shown in Table 1 into Eq. (13) yielded the relationship between the u and the $A_{p\text{-}p}$ as shown in Fig. 16. It can be seen from this figure that although the specific grinding energy u varied between u_L and u_H at the given $A_{p\text{-}p}$ for the sake of the ultrasonic vibration, the u intended to decrease as the $A_{p\text{-}p}$ increases, confirming that the ultrasonication benefits the reduction in the specific grinding energy significantly.

5 Conclusions

The chip formation in UAG of Inconel 718 using electroplated cBN grinding wheel was investigated in terms of chips size, chip geometry, and grinding forces for different ultrasonic vibration amplitudes and wheel peripheral speeds. The obtained results can be summarized as the followings:

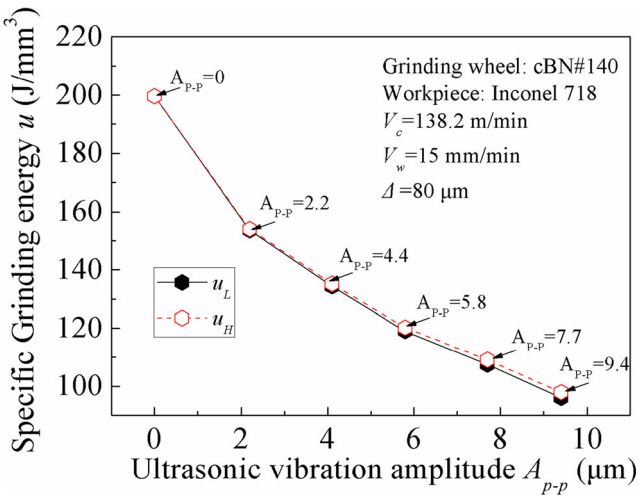

Fig. 16 Effects of vibration amplitude on specific grinding energy

(1) The chip size, i.e., cross-section area and length, is distinctly affected by the ultrasonication but little effect of wheel peripheral speed is observed;
(2) The UAG is potentially avoiding the formation of shear chips and prefers the flow chips especially at larger amplitude;
(3) In CG without ultrasonication the wheel peripheral speed would affect the chip formation significantly, whereas in UAG the chip formation is hardly affected by the speed.
(4) In UAG at the ultrasonic vibration amplitude of $A_{p\text{-}p}$= 9.4 μm, the normal and tangential grinding forces were smaller by 42.5 and 40 %, respectively, compared to those in CG, when the wheel peripheral speed was 138.2 m/min.
(5) The specific grinding energy u in UAG is smaller than that in CG and intended to decrease as the $A_{p\text{-}p}$ increases, demonstrating that the ultrasonication benefits the reduction in the specific grinding energy.

Acknowledgments A part of this work was conducted collaboratively with Taruishi Kikou Co., Ltd. under the financial support of Akita Prefectural manufacturing technology promotion fund.

References

1. Sharman A, Dewes RC, Aspinwall DK (2001) Tool life when high speed ball nose end milling Inconel 718. J Mater Process Technol 118:29–35. doi:10.1016/S0924-0136(01)00855-X
2. Radhakrishna CH, Prasad Rao K (1997) The formation and control of laves phase in superalloy 718 welds. J Mater Sci 32:1977–1984. doi:10.1023/A:1018541915113
3. Ezugwu EO, Fadare DA, Bonney J, Da Silva RB, Sales WF (2005) Modelling the correlation between cutting and process parameters in high-speed machining of inconel 718 alloy using an artificial neural network. Int J Mach Tools Manuf 45:1375–1385. doi:10.1016/j.ijmachtools.2005.02.004
4. Arunachalam M, Mannan MA, Spowage AC (2004) Surface integrity when machining age hardened inconel 718 with coated carbide cutting tools. Int J Mach Tools Manuf 44:1481–1491. doi:10.1016/j.ijmachtools.2004.05.005
5. Ulutan D, Ozel T (2011) Machining induced surface integrity in titanium and nickel alloys: a review. Int J Mach Tools Manuf 51: 250–280. doi:10.1016/j.ijmachtools.2010.11.003
6. Khidhir BA, Mohamed B (2010) Machining of nickel based alloys using different cemented carbide tools. J Eng Sci Technol 5(3):264–271
7. Arunachalam RM, Mannan MA, Spowage AC (2004) Residual stress and surface roughness when facing age hardened Inconel

718 with CBN and ceramic cutting tools. Int J Mach Tools Manuf 44:879–887. doi:10.1016/j.ijmachtools.2004.02.016
8. Ozcelik B, Oktem H, Kurtaran H (2005) Optimum surface roughness in end milling inconel 718 by coupling neural network model and genetic algorithm. Int J Adv Manuf Technol 27:234–241. doi:10.1007/s00170-004-2175-7
9. Kitagawa T, Kubo A, Maekawa K (1997) Temperature and wear of cutting tools in high-speed machining of inconel 718 and Ti-6Al-6V-2Sn. Wear 202:142–148. doi:10.1016/S0043-1648(96)07255-9
10. Shokrani A, Dhokia V, Newman ST (2012) Environmentally conscious machining of difficult-to- machine materials with regard to cutting fluids. Int J Mach Tools Manuf 57:83–101. doi:10.1016/j.ijmachtools.2012.02.002
11. Santosh Ranganath, Changsheng Guo, Sean Holt (2009) Experimental Investigations Into the Carbide Cracking Phenomenon on Inconel 718 Superalloy Material, ASME 2009 International Manufacturing Science and Engineering Conference Volume 2:33–39. doi:10.1115/MSEC2009-84085
12. Zemzemi F, Rech J, Ben Salem W, Dogui A, Kapsa P (2014) Identification of friction and heat partition model at the tool-chip-workpiece interfaces in dry cutting of an Inconel 718 alloy with CBN and coated carbide tools. Adv Manuf Sci Technol 38(1):5–22. doi:10.2478/amst-2014-0001
13. Ohkubo C, Toshio H, Phillip Ford J, Watanabe I (2006) Effect of surface reaction layer on grindability of cast titanium alloys. Dent Mater 22(3):268–274. doi:10.1016/j.dental.2005.04.020
14. Irani RA, Bauer RJ, Warkentin A (2005) A review of cutting fluid application in the grinding process. Int J Mach Tools Manuf 45:1696–1705. doi:10.1016/j.ijmachtools.2005.03.006
15. Liu JH, Pei ZJ, Fisher GR (2007) Grinding wheels for manufacturing of silicon wafers: a literature review. Int J Mach Tools Manuf 47:1–13. doi:10.1016/j.ijmachtools.2006.02.003
16. Brehl DE, Dow TA (2008) Review of vibration-assisted machining. Precis Eng 32:153–172. doi:10.1016/j.precisioneng.2007.08.003
17. Pei Z, Ferreira P (1998) Modeling of ductile-mode material removal in rotary ultrasonic machining, Int. J Mach Tools Manuf 38:1399–1418. doi:10.1016/S0890-6955(98)00007-8
18. Jianguo C, Yongbo W, Dong L, Masakazu F, Mitsuyoshi N (2014) Material removal behavior in ultrasonic-assisted scratching of SiC ceramics with a single diamond tool. Int J Mach Tools Manuf 79:49–61. doi:10.1016/j.ijmachtools.2014.02.002
19. Bhaduri D, Soo SL, Aspinwal DK (2012) A study on ultrasonic assisted creep feed grinding of nickel based superalloys. Procedia CIRP 1:359–364. doi:10.1016/j.procir.2012.04.064
20. Bhaduri D, Soo SL, Novovic D, Aspinwall DK, Harden P, Waterhouse C (2013) Ultrasonic assisted creep feed grinding of inconel 718. Procedia CIRP 6:616–621. doi:10.1016/j.procir.2013.03.044
21. Zahedi A, Tawakoli T, Akbari J (2015) Energy aspects and workpiece surface characteristics in ultrasonic assisted cylindrical grinding of alumina-zirconia ceramics. Int J Mach Tools Manuf 90:16–28. doi:10.1016/j.ijmachtools.2014.12.002
22. Tso P-L, Wu S-H (1990) Analysis of grinding quantities through chip sizes. J Mater Process Technol 95:1–17. doi:10.1016/S0924-0136(99)00297-6
23. Lu L, Farris TN, Chandrasekar S (1992) Paper VI (iv) sliding microindentation wear particles: spheres in grinding swarf. Tribology Series 21:257–263. doi:10.1016/S0167-8922(08)70531-5
24. Jianbo D, Wenfeng D, Liangchi Z, Jiuhua X, Honghua S (2015) Understanding the effects of grinding speed and undeformed chip thickness on the chip formation in high-speed grinding. Int J Adv Manuf Technol 81(5):995–1005. doi:10.1007/s00170-015-7265-1
25. Milton C. Shaw (1996) Principles of abrasive processing, Mech. Chem. Engng., Inst. Engrs, Australia MC8, 73
26. Salje E, Mohlgan H (1986) Fundamental dependencies upon contact lengths and results in grinding. CIRP Ann Manuf Technol 35(1):249–253. doi:10.1016/S0007-8506(07)61881-2
27. Ioan D. Marinescu Mike P. Hitchiner, Eckart Uhlmann W. Brian Rowe Ichiro Inasak (2006) Handbook of Machining with Grinding Wheels, CRC Press, Technology & Engineering:632 ISBN: 978-1-57444-671-5
28. Taghi T, Bahman A, Mohammad R (2009) Ultrasonic assisted dry grinding of 42CrMo4. Int J Adv Manuf Technol 42:883–891. doi:10.1007/s00170-008-1646-7
29. Tso P-L (1995) An investigation of chip types in grinding. J Mater Process Technol 53:521–532. doi:10.1016/0924-0136(94)01746-N
30. Wu YB, Nomura M, Feng ZJ, Kato M (2004) Modeling of grinding force in constant-depth-of-cut ultrasonically assisted grinding. Mater Sci Forum 471–472:101–106. doi:10.4028/www.scientific.net/MSF.471-472.101
31. Teidelt E, Starcevic J, Popov VL (2012) Influence of ultrasonic oscillation on static and sliding friction. Tribol Lerr 48:51–62. doi:10.1007/s11249-012-9937-4
32. Park CH, Inman DJ (2003) Enhanced piezoelectric shunt design. Shock Vib 10(2):127–133. doi:10.1155/2003/863252
33. Aslan D, Budak E (2015) Surface roughness and thermo-mechanical force modeling for grinding operations with regular and circumferentially grooved wheel. Int J Mach Tools Manuf 223:75–90. doi:10.1016/j.jmatprotec.2015.03.023
34. Liang Z, Wu Y, Wang X, Zhao W (2010) A new two-dimensional ultrasonic assisted grinding (2D-UAG) method and its fundamental performance in monocrystal silicon machining. Int J Mach Tools Manuf 5(8):728–736. doi:10.1016/j.ijmachtools.2010.04.005
35. Griffith B (2001) Manufacturing, surface technology-surface integrity and functional performance. Penton Press, London
36. Armarego EJ, Brown RH (1969) The machining of metals. Prentice-Hall, Englewood Cliffs, New Jersey
37. Park HW (2008) Development of micro-grinding mechanics and machine tools. Georgia Institute of Technology, United States
38. Zhang DK, Li C, Jia D, Zhang Y (2014) Investigation into engineering ceramics grinding mechanism and the influential factors of the grinding force. Int J Control Autom 7(4):19–34. doi:10.14257/ijca.2014.7.4.03